

pubs.acs.org/JACS Article

High-Concentration Self-Assembly of Zirconium- and Hafnium-Based Metal-Organic Materials

Ronald T. Jerozal, Tristan A. Pitt, Samantha N. MacMillan, and Phillip J. Milner*



Cite This: J. Am. Chem. Soc. 2023, 145, 13273-13283



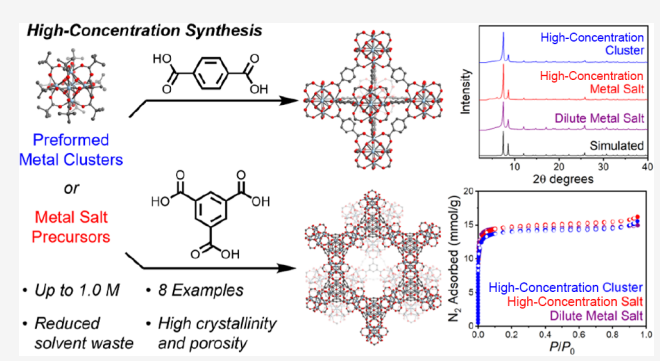
ACCESS

III Metrics & More

Article Recommendations

s Supporting Information

ABSTRACT: Metal—organic frameworks (MOFs) are crystalline, porous solids constructed from organic linkers and inorganic nodes that are promising for applications in chemical separations, gas storage, and catalysis, among many others. However, a major roadblock to the widespread implementation of MOFs, including highly tunable and hydrolytically stable Zr- and Hf-based frameworks, is their benchtop-scalable synthesis, as MOFs are typically prepared under highly dilute (≤0.01 M) solvothermal conditions. This necessitates the use of liters of organic solvent to prepare only a few grams of MOF. Herein, we demonstrate that Zr- and Hf-based frameworks (eight examples) can self-assemble at much higher reaction concentrations than are typically utilized, up to 1.00 M in many cases. Combining stoichiometric amounts of Zr



or Hf precursors with organic linkers at high concentrations yields highly crystalline and porous MOFs, as confirmed by powder X-ray diffraction (PXRD) and 77 K N_2 surface area measurements. Furthermore, the use of well-defined pivalate-capped cluster precursors avoids the formation of ordered defects and impurities that arise from standard metal chloride salts. These clusters also introduce pivalate defects that increase the exterior hydrophobicity of several MOFs, as confirmed by water contact angle measurements. Overall, our findings challenge the standard assumption that MOFs must be prepared under highly dilute solvothermal conditions for optimal results, paving the way for their scalable and user-friendly synthesis in the laboratory.

■ INTRODUCTION

Metal-organic frameworks (MOFs) are crystalline, porous materials composed of inorganic nodes bridged by organic linkers. Their permanent porosity, large number of accessible topologies, and tunable pore environments make MOFs appealing platforms for applications in gas storage, chemical separations, catalysis, and beyond.^{2–4} A major roadblock to the further development of MOFs is their synthesis on a laboratory-scale (1-100 g), especially by nonspecialists such as medicinal chemists. 5,6 This is because many MOFs are synthesized under highly dilute (≤ 0.01 M) solvothermal conditions using toxic N,N-dimethylformamide (DMF) as the solvent, which results in significant waste and necessitates the use of liters of solvent to prepare only a few grams of MOF. Although the volume of organic solvent can be reduced using mechanochemistry,⁵⁻⁹ this approach requires specialized equipment such as ball mills or screw extruders, which are inaccessible to many researchers. A more user-friendly approach would be to simply conduct solvothermal synthesis at much higher reaction concentrations (e.g., 1.00 M, an approximately 100-fold increase). 10,111 However, examples of successful MOF syntheses even at intermediate concentrations (0.15-0.25 M) remain surprisingly scarce; ^{10,12-15} more common instead are reports of poorly crystalline products, unusual morphologies, low surface area materials, or different

phases forming at high concentrations due to the rapid precipitation of products from solution. These findings beg the question: Can MOFs effectively self-assemble at high reaction concentrations?

MOFs constructed from Zr_6 nodes (Zr-MOFs), $^{20-22}$ as well as isostructural Hf-based MOFs (Hf-MOFs), 23 exemplify the challenges and opportunities associated with high-concentration MOF synthesis. These frameworks represent a privileged class of materials due to their structural tunability, hydrothermal stability, biocompatibility, and catalytic activity. $^{20,21,24-26}$ However, Zr-MOFs are typically prepared under highly dilute solvothermal conditions in DMF. Furthermore, many Zr-MOF syntheses require a large excess (>50 equiv) of exogenous acid modulators, which improve the reversibility of MOF self-assembly (leading to more crystalline products) at the cost of drastically increasing the amount of waste associated with MOF synthesis. $^{27-29}$ Additionally, an excess

Received: March 16, 2023 Published: June 9, 2023





of either the linker or Zr precursor is often used. Mechanochemical methods, such as liquid-assisted grinding (LAG), have been used to synthesize several Zr-MOFs, including UiO-66 (UiO = Universitetet i Oslo), UiO-66-NH₂, UiO-67, and NU-901 (NU = Northwestern University). 30-36 In addition to requiring specialized equipment, mechanochemical Zr-MOF syntheses generally utilize preformed Zr oxo clusters prepared from water-sensitive Zr alkoxides and capped by acetate or methacrylate groups, with different precursors and grinding liquids employed to access specific frameworks. The MOFs produced by mechanochemical synthesis also vary in crystallinity, with broad powder X-ray diffraction (PXRD) reflections indicative of small crystalline domain sizes in many cases.^{34–36} On the other hand, the highconcentration solvothermal synthesis of UiO-66 (~0.45 M) has only been achieved when the reaction mixture was seeded with pre-synthesized MOF, 10 and successful high-concentration synthesis (>0.25 M) has yet to be reported for any other Zr- or Hf-MOF.

Herein, we demonstrate that high-quality Zr- and Hf-MOFs can be generally synthesized at high reaction concentrations, up to 1.00 M in linker in many cases, using either simple metal chloride salts or well-defined pivalate-capped cluster precursors. This includes six MOFs with 12-connected nodes (UiO-66, UiO-66(Hf), UiO-66-NH₂, UiO-66-(OH)₂, UiO-67, and UiO-68-Me₂), as well as mesoporous MOFs with eightconnected (PCN-128, PCN = porous coordination network) and six-connected (MOF-808) nodes. Additionally, the correct stoichiometric ratios between the linker and metal can be employed without the need for excess organic acid in most cases. This user-friendly approach toward the benchtop-scale synthesis of Zr- and Hf-MOFs challenges the widespread assumption that high-quality MOFs can only be prepared under dilute conditions, paving the way for the straightforward synthesis of MOFs by any researcher.

RESULTS AND DISCUSSION

Cluster Precursor Selection and Synthesis. Typical solvothermal syntheses of Zr-MOFs employ Zr salt precursors (e.g., ZrCl₄, ZrOCl₂:xH₂O), which first self-assemble into Zr oxo clusters in the presence of water and then combine with the linkers to yield extended MOF structures.³⁷ However, previous mechanochemical approaches have exclusively used pre-formed Zr oxo clusters to obtain the desired MOF,³ indicating that node self-assembly may be problematic in some cases. To interrogate whether node self-assembly affects MOF formation under high-concentration conditions, we aimed to evaluate carboxylate-capped Zr oxo clusters alongside simple Zr salts as MOF precursors. Zr oxo clusters with varying structures and capping ligands have been reported, among which tetranuclear (Zr₄), hexanuclear (Zr₆), and dodecanuclear clusters (Zr₁₂) are the most common (Supporting Information or SI Figure S7).³⁹ The Zr₆ methacrylate $(Zr_6O_4(OH)_4(MA)_{12}, MA^- = methacrylate)$ and Zr_{12} acetate $([Zr_6O_4(OH)_4(OAc)_{12}]_2, OAc^- = acetate)$ clusters, referred to herein as Zr₆ MA and Zr₁₂ OAc, respectively, have proven to be the most effective precursors for mechanochemical Zr-MOF synthesis. 32-34 Additionally, preformed clusters capped with MA or OAc have been used to enable the room-temperature synthesis of some Zr MOFs under dilute reaction conditions. 40,41 However, Zr₆ MA generates toxic methacrylic acid and polymeric impurities upon MOF formation and thus was avoided in this work.32

The ability of Zr₁₂ OAc to serve as a precursor for the synthesis of UiO-66 under high-concentration solvothermal conditions was first evaluated (see SI Section 5 for details). Unfortunately, poorly crystalline material was obtained (SI Figure S8). This is likely due to the differing structures of the Zr₁₂ OAc cluster and the Zr₆ node of UiO-66, leading to a complex mixture of products. The distinct Zr clusters do not necessarily interconvert upon undergoing ligand exchange in solution, especially the inter-cluster bridging carboxylates of the two dimerized Zr₆ clusters that make up the Zr₁₂ dimer. 42,43 Furthermore, while some mechanochemical and solvothermal MOF syntheses have achieved in situ Zr₁₂ to Zr₆ cluster transitions, a number of MOFs with Zr₁₂ nodes, including some synthesized from Zr₁₂ OAc, have also been reported. 44-47 As such, we set out to identify a user-friendly Zr₆ cluster—ideally that could be synthesized without the use of water-sensitive Zr alkoxides—to serve as a high-concentration MOF precursor.

Previous reports indicate that α -branching on the capping carboxylic acid favors the formation of Zr₆ clusters over other possible structures.^{39,42,48} Hypothesizing that very bulky capping carboxylates should enforce the correct node architecture, we identified the pivalate-capped cluster $Zr_6O_4(OH)_4(OPiv)_{12}$ (OPiv = pivalate), referred to herein as ZrPiv, as a promising yet hitherto unexplored potential MOF precursor.⁴⁹ Simply combining ZrCl₄, pivalic acid (PivOH), and DMF under solvothermal conditions yielded large crystals of ZrPiv (see SI Section 4 for details). Singlecrystal X-ray diffraction (SCXRD) confirmed that ZrPiv possesses the same Zr₆ cluster as UiO-66 (Figure 1b and see

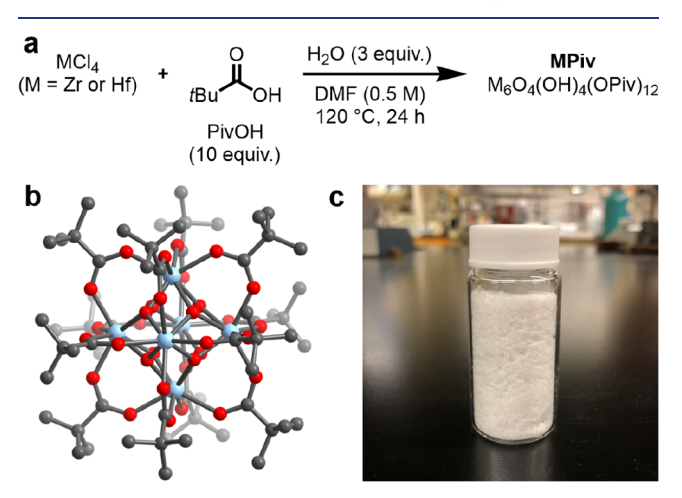


Figure 1. (a) High-concentration solvothermal synthesis of MPiv (M = Zr, Hf). (b) SCXRD structure of ZrPiv. The gray, red, and light blue spheres represent carbon, oxygen, and zirconium, respectively. Hydrogens are omitted for clarity. (c) Twelve grams of ZrPiv from a single-batch synthesis.

SI Section 17). The structure of ZrPiv differs from that of all other reported molecular Zr₆ clusters, as the carboxylates are all in bridging coordination modes—mirroring the MOF—and there are no co-crystallized solvent or carboxylic acid molecules. The optimal high-concentration conditions using 10 equiv of PivOH relative to ZrCl₄ (Figure 1a) allowed for the rapid synthesis of over 12 g of highly crystalline ZrPiv in a single batch (Figure 1c). This facile solvothermal method could be extended to the previously unreported Hf analogue, Hf₆O₄(OH)₄(OPiv)₁₂, referred to herein as HfPiv. SCXRD

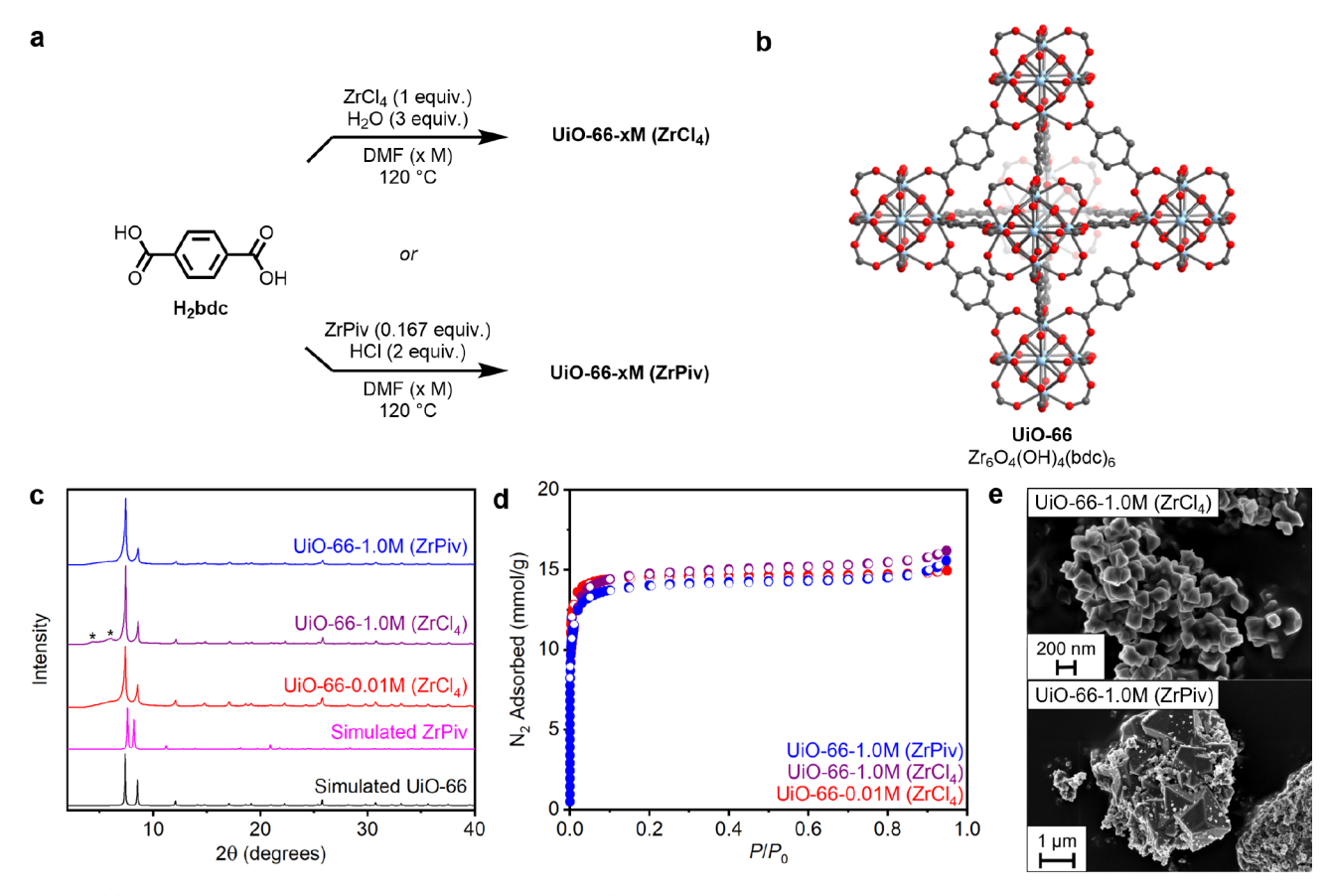


Figure 2. (a) Synthesis of UiO-66 from either $ZrCl_4$ or ZrPiv. (b) The structure of UiO-66. Gray, red, and light blue spheres represent carbon, oxygen, and zirconium, respectively. Hydrogens are omitted for clarity. (c) PXRD patterns of UiO-66 samples prepared using $ZrCl_4$ or ZrPiv and a $[H_2bdc]$ of either 0.01 or 1.0 M. The simulated patterns based on the SCXRD structures of ZrPiv and UiO-66 are included for reference. The asterisks indicate reflections from crystalline domains of ordered missing node defects with a **reo** topology. (d) N_2 adsorption (filled circles) and desorption (open circles) isotherms of the activated UiO-66 samples. (e) SEM images of the high-concentration UiO-66 samples from either precursor.

confirmed that HfPiv is isostructural to ZrPiv (SI Figure S140, SI Section 17). High-concentration conditions allowed for the rapid synthesis of over 6 g of HfPiv in a single batch. In both cases, no other cluster geometries were observed in bulk PXRD measurements. As such, ZrPiv and HfPiv are promising potential precursors for the synthesis of Zr- and Hf-based MOFs with pre-assembled $\rm M_6$ nodes.

High-Concentration Synthesis of UiO-66. Traditional solvothermal Zr-MOF synthesis involves the combination of a Zr salt or pre-formed cluster, organic linker, solvent (typically DMF), water (to facilitate node formation), and acid modulator (10-50 equiv) at high temperatures (120 °C) for extended periods of time (24-72 h).⁵⁰ We aimed to employ stoichiometric linker:metal ratios and avoid acid modulators where possible to minimize the unnecessary waste associated with Zr-MOF synthesis. Reduced solvent volumes also allow for the use of simple reaction vessels, as opposed to more specialized glassware such as Teflon autoclaves. After synthesis, MOFs were soaked in appropriate organic solvents to remove soluble impurities, as is standard practice for MOF synthesis, ⁵¹ followed by characterization using PXRD, infrared (IR) spectroscopy, scanning electron microscopy (SEM), thermogravimetric analysis (TGA), and surface area analysis.

We first investigated whether the archetypical Zr-MOF UiO-66 can self-assemble under high-concentration conditions using either ZrCl₄ or ZrPiv as the Zr source (Figure 2). ^{10,52} A 1:1 ratio of ZrCl₄ and the linker terephthalic acid (H₂bdc) were combined with increasing concentrations in DMF (x M with respect to the linker) with stirring to yield samples labeled as UiO-66-xM (ZrCl₄) (Figure 2a, see SI Section 5 for details). Additional water (3 equiv) was added to all syntheses involving ZrCl₄ to facilitate node assembly, as the adventitious water in DMF was not sufficient to achieve this at high reaction concentrations. In contrast to a literature report, 10 samples prepared up to 1.0 M in DMF yielded UiO-66 with comparable crystallinity to material prepared at the standard concentration of 0.01 M (Figure 2c). PXRD analysis revealed that the high-concentration samples possess crystalline nanoregions of ordered missing node defects with a reo topology (SI Figure S12).⁵³ Previous work demonstrated that the number of missing node defects increases with increasing acid modulator concentration, decreasing reaction pH and decreasing linker:metal ratios. 53,54 In addition, these nanodomains were observed for the intermediate concentration (0.20 M) synthesis of Zr-halofumarate frameworks due to the acid released upon the hydrolysis of ZrX_4 (X = Cl, Br, or I) salts.⁵⁵ Thus, the ordered defect nanoregions in high-concentration UiO-66 likely arise from the excess HCl generated in situ from the hydrolysis of ZrCl₄.²

In contrast to previous solvothermal methods using preformed cluster precursors, 40,41 combining ZrPiv with H_2bdc directly under the standard reaction conditions did

not produce UiO-66 (SI Figure S13), potentially due to its poor solubility in DMF. The addition of concentrated HCl (1 equiv per pivalate) was found to facilitate exchange of the capping pivalates for linkers, leading to highly crystalline UiO-66 (Figure 2c). Notably, the reaction of ZrPiv with HCl in the absence of linker yielded poorly crystalline ZrPiv, indicating that the role of HCl is largely to promote carboxylate exchange and not to decompose ZrPiv into simpler Zr species (SI Figures S17 and S18). A stoichiometric 1:6:12 ratio of ZrPiv:H₂bdc:HCl was combined in varying amounts of DMF with increasing concentrations (x M with respect to the linker) to synthesize MOF samples labeled as UiO-66-xM (ZrPiv) (Figure 2a, see SI Section 5 for details). Similar to the results obtained with ZrCl₄, UiO-66-1.0 M (ZrPiv) possesses comparable crystallinity to MOF prepared under dilute conditions (Figure 2b). Notably, samples prepared from ZrPiv at high concentrations did not display additional lowangle reflections corresponding to ordered missing cluster defects. Although the ZrPiv-derived samples lack these topological impurities, longer reaction times (72 h) are needed to fully convert ZrPiv into MOF, likely due to the need for carboxylate exchange at the node (SI Figure S15). In contrast, crystalline UiO-66 was obtained after only 1 h when using ZrCl₄ and high-concentration conditions (SI Figure S10). These results highlight the suitability of Zr-MOFs to be synthesized at high concentrations. We propose that the high stability of the Zr₆ node and the strength of the Zr-O bonds formed provide the driving force to self-assemble efficiently regardless of the high reaction concentrations. Further aging of this concentrated mixture allows for the dynamic ligand exchange (albeit slow due to the strong Zr-O bonds) crucial to the formation of crystalline frameworks.²⁷ In particular, this is demonstrated by the exchange of the initial capping pivalates for linkers during the high-concentration synthesis using ZrPiv.

To further characterize the quality of the high-concentration UiO-66 samples, their porosity was assessed via 77 K N₂ adsorption/desorption isotherms (Figure 2d). From these isotherms, the Brunauer-Emmett-Teller (BET) surface areas were determined to be 1327 ± 8 and 1232 ± 7 m²/g for UiO-66-1.0 M (ZrCl₄) and UiO-66-1.0 M (ZrPiv), respectively. These values are comparable to previously reported BET surface areas for UiO-66 (800-1800 m²/g, depending on defect concentration) and to a sample of UiO-66 prepared at a linker concentration of 0.01 M (1341 \pm 4 m²/g). Pore-size distributions for both of the 1.0 M samples (SI Figure S21) revealed the presence of larger micropores, consistent with the presence of missing-cluster defects. Additionally, the pore volumes of both 1.0 M samples (SI Table S1) were greater than the calculated pore volume of UiO-66. Together, these indicate that despite UiO-66-1.0 M (ZrPiv) not displaying additional PXRD reflections from ordered defects, as UiO-66-1.0 M (ZrCl₄) does, the two samples contain similar amounts of defects. SEM images of the high-concentration samples revealed slight differences between the two Zr precursors as well (Figure 2e). The 1.0 M sample prepared using ZrCl₄ consists of aggregates of small crystallites and not the welldefined octahedra typical of UiO-66.²⁹ Conversely, the ZrPiv sample led to a mixture of small particles and aggregates of larger crystallites exhibiting well-defined edges, indicative of incompletely formed octahedra. This range of crystallite sizes persisting despite thorough solvent washing indicates that this high-concentration method does not provide narrow particle size distributions such as those observed in modulated

syntheses.²⁷ The IR spectra (SI Figures S27 and S33) and the TGA decomposition profiles (SI Figures S26 and S32) of both high-concentration samples were comparable. Together, these findings support that high-concentration solvothermal synthesis is suitable for preparing crystalline, porous UiO-66 from either a Zr salt or a pre-formed Zr cluster precursor.

Competing carboxylates, including formate from the in situ hydrolysis of DMF, can be incorporated as linker substitution defects in MOFs.²⁹ To further interrogate potential differences between the MOFs prepared from ZrCl₄ and ZrPiv, the degree of pivalate defect incorporation in UiO-66-1.0 M (ZrPiv) was assessed. Linker deficiencies and modulator incorporation can be quantified by ¹H NMR spectroscopy of acid- or basedigested samples (see SI Section 2 for details). 27,54,57 1H NMR analysis of digested UiO-66-1.0 M (ZrPiv) (SI Figure S31) revealed a OPiv-:bdc2- ratio of 0.11:1, which is comparable to previous dilute solvothermal syntheses of UiO-66 using a slight excess of competing monocarboxylic acid modulators. 54 When UiO-66-1.0 M (ZrCl₄) was synthesized in the presence of two equiv. of PivOH—the same amount of pivalate present in the synthesis using ZrPiv—a OPiv-:bdc²⁻ ratio of 0.04:1 was obtained (SI Figure S20). Thus, using ZrPiv as a precursor leads to higher carboxylate incorporation than traditional acid modulation does.²⁹

The presence of defects has been shown to greatly impact the properties of Zr-MOFs. 13,58 We hypothesized that the nonpolar pivalate defects present in UiO-66-1.0 M (ZrPiv) should impart the MOF with improved hydrophobicity. Indeed, UiO-66-1.0 M (ZrPiv) floats on water, yet UiO-66-1.0 M (ZrCl₄) is rapidly wetted (Figure 3a inset). The

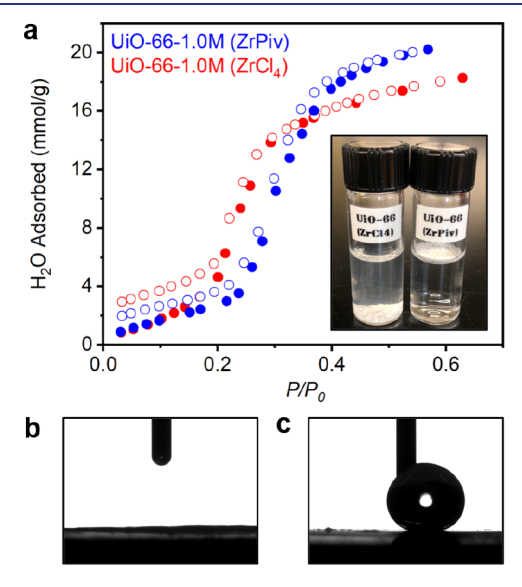


Figure 3. (a) Water vapor adsorption isotherms of high-concentration UiO-66 samples. Inset: UiO-66-1.0 M (ZrCl₄) (left) sinking in water, in contrast to UiO-66-1.0 M (ZrPiv) (right) floating on water. Water contact angle measurements of (b) UiO-66-1.0 M (ZrCl₄) and (c) UiO-66-1.0 M (ZrPiv).

crystallographic density of UiO-66 (1.24 g/cm³) is greater than that of water, suggesting that UiO-66-1.0 M (ZrPiv) must have a hydrophobic exterior in contrast to the hydrophilic exterior of UiO-66-1.0 M (ZrCl₄). Water contact angle measurements (see SI Section 15 for details)—which quantify the wettability of a surface by measuring the contact angle of the water droplet formed after addition of water to a material—

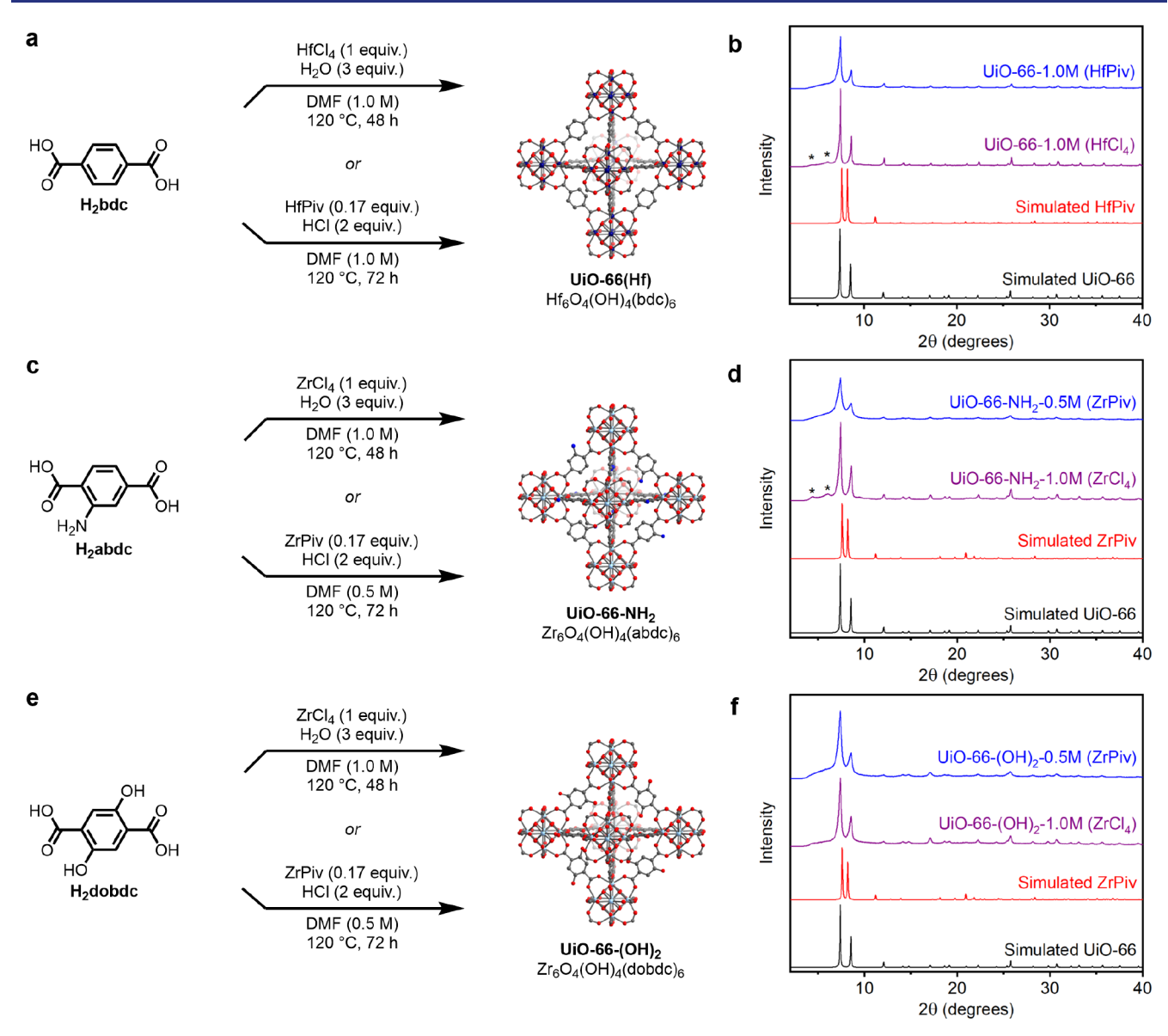


Figure 4. High-concentration syntheses of (a) UiO-66(Hf), (c) UiO-66-NH₂, and (e) UiO-66-(OH)₂ from either MCl₄ or MPiv (M = Zr or Hf). The gray, red, blue, dark blue, and light blue spheres represent carbon, oxygen, nitrogen, hafnium, and zirconium, respectively. Hydrogens are omitted for clarity. PXRD patterns of (b) UiO-66(Hf), (d) UiO-66-NH₂, and (f) UiO-66-(OH)₂ samples prepared at high concentration from either precursor. The simulated patterns based on the SCXRD structures of ZrPiv and UiO-66 are included for reference. The asterisks indicate reflections from crystalline domains of ordered missing node defects with a **reo** topology. The asterisks indicate reflections from crystalline domains of ordered missing node defects with a **reo** topology.

confirmed that UiO-66-1.0 M (ZrCl₄) has a hydrophilic surface with a contact angle of 0° (Figure 3b). In contrast, water dropped on the surface of UiO-66-1.0 M (ZrPiv) forms a droplet with a large contact angle of 162° (Figure 3c), indicating that it has a super-hydrophobic surface. The external surface hydrophobicity of MOFs is not necessarily representative of their internal surface properties. 59,60 Thus, 303 K water vapor adsorption isotherms were also measured to determine the relative pressures at which half of the total water capacities are reached (α) (Figure 3a), in which a larger α indicates weaker interactions between the pore and adsorbed water.⁶¹ Both high-concentration samples display a type V water adsorption isotherm, consistent with previous reports. 61,62 For UiO-66-1.0 M (ZrPiv), $\alpha = 0.30$, indicating that it has a more hydrophobic interior than UiO-66-1.0 M (ZrCl₄) ($\alpha = 0.24$). Overall, these findings demonstrate that well-defined Zr cluster precursors can incorporate capping ligands as defects that alter

the physical properties of the resulting materials. As such, this approach enables defect engineering without the need to add a large excess of carboxylic acid during MOF synthesis.

Generality of High-Concentration MOF Synthesis. To evaluate the scope of high-concentration solvothermal MOF synthesis, we prepared an isoreticular series of frameworks that share the same fcu topology and structure as UiO-66, including the Hf analogue of UiO-66, ²³ the amine-function-alized UiO-66-NH₂, ⁶³ and the dihydroxy-functionalized UiO-66-(OH)₂, also known as MOF-804, at high reaction concentrations (Figure 4, SI Sections 7, 8, and 9). ¹³ Both ZrCl₄ and ZrPiv were assessed as MOF precursors, given the different outcomes observed for UiO-66. In general, MOF formation was complete in 48 h using ZrCl₄ but required 72 h with ZrPiv. The synthesis of each MOF was evaluated at concentrations of 0.5 and 1.0 M for comparison, and further

characterization was carried out on the samples successfully prepared at the highest tested concentration.

UiO-66(Hf) is an intriguing MOF for X-ray computed tomography imaging and radiotherapeutic applications. 64,65 The results of the high-concentration syntheses of UiO-66(Hf) mirror those observed for UiO-66(Zr) (Figure 4a). For both HfCl₄ and HfPiv, highly crystalline MOF was obtained at a linker concentration of 1.0 M (Figure 4b). The MOF prepared from HfCl₄ contained detectable, ordered missing cluster defects, 53 whereas the MOF prepared from HfPiv did not. 77 K N₂ adsorption/desorption isotherms revealed that the BET surface areas of UiO-66-1.0 M (HfCl₄) and UiO-66-1.0 M (HfPiv) are 961 \pm 6 and 988 \pm 7 m²/g, respectively (Figure 5), which are in agreement with the range of reported values

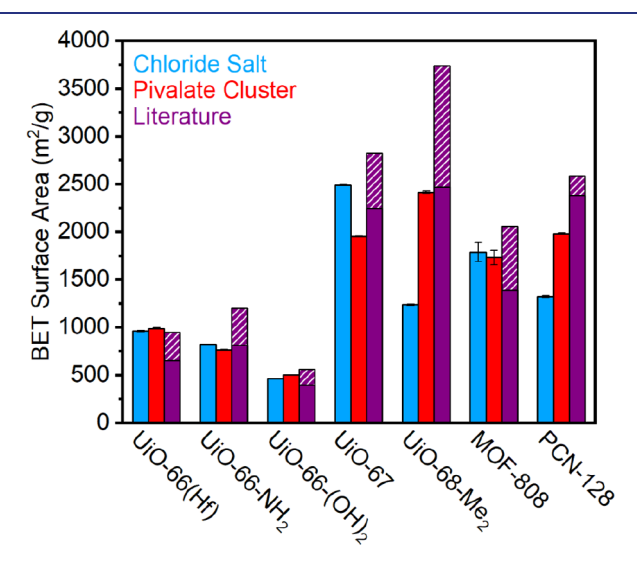


Figure 5. 77 K N_2 Brunauer–Emmett–Teller (BET) surface areas of MOFs prepared at high-concentrations using either M chloride salt or MPiv (M = Zr or Hf) precursors, as compared to reported literature values. The shaded regions represent the range of reported BET surface areas. $^{13,28,32,34,66-72,76,77}$

(655–950 m²/g). 66,67 Similar to UiO-66(Zr), the pore size distributions (SI Figures S35 and S42) and pore volumes (SI Table S1) indicate that both UiO-66(Hf) samples contain similar amounts of defects leading to increased overall pore sizes. ¹H NMR of digested UiO-66-1.0 M (HfPiv) (SI Figure S45) revealed a OPiv⁻:bdc²⁻ ratio of 0.17:1. Similar to UiO-66(Zr), these OPiv⁻ defects increased the hydrophobicity of the material, such that UiO-66-1.0 M (HfPiv) has a superhydrophobic exterior with a contact angle of 154°, in contrast to the hydrophilic surface of UiO-66-1.0 M (HfCl₄) (SI Figure S137). These findings support that the high-concentration syntheses of Zr-MOFs can be readily extended to their Hf analogues.

The suitability of high-concentration solvothermal synthesis for preparing substituted UiO-66 analogues was next evaluated. Aminoterephthalic acid (H₂abdc) was combined with either ZrCl₄ or ZrPiv at high concentrations in DMF to yield UiO-66-NH₂ (Figure 4c). Similar to UiO-66, the use of ZrCl₄ as a precursor led to highly crystalline UiO-66-NH₂—with ordered missing node defects—at linker concentrations as high as 1.0 M (Figure 4d). With ZrPiv, linker concentrations of 0.5 M led to crystalline MOF but a concentration of 1.0 M resulted in significant impurity from unreacted ZrPiv, even after 72 h (SI Figure SSS). The high-concentration synthesis of UiO-66-

(OH)₂ revealed similar results, in that ZrCl₄ allowed for the synthesis of crystalline MOF at a higher concentration than ZrPiv (Figure 4e,f). The overall pore volume is decreased in these functionalized frameworks compared to UiO-66, which likely impedes linker/pivalate exchange at very high concentrations. Nonetheless, the BET surface areas for UiO-66-NH₂-1.0 M (ZrCl₄) and UiO-66-NH₂-0.5 M (ZrPiv) were 822 \pm 2 and 765 ± 2 m²/g, respectively (Figure 5), which are comparable to the range of literature values (815-1200 m²/ g). 28,32 Likewise, the BET surface areas of both highconcentration UiO-66-(OH)₂ samples were in agreement with reported values $(464-560 \text{ m}^2/\text{g})$, with UiO-66- $(OH)_2$ -0.5 M (ZrPiv) possessing a slightly higher BET surface area of 503 ± 2 m²/g compared to 464 ± 1 m²/g for UiO-66-(OH)₂- 1.0 M (ZrCl₄) (Figure 5). ^{28,68} The pore size distributions of $UiO-66-NH_2-0.5$ M (ZrPiv) and $UiO-66-(OH)_2-0.5$ M (ZrPiv) (SI Figures S56 and S70) display larger micropores than the corresponding ZrCl₄ prepared MOFs (SI Figures S49 and S63). ¹H NMR analysis of digested UiO-66-NH₂-0.5 M (ZrPiv) and UiO-66-(OH)₂-0.5 M (ZrPiv) indicates that both contain significant OPiv defects (SI Figures S59 and S73). Consistently, UiO-66-NH₂-0.5 M (ZrPiv) displayed increased surface hydrophobicity compared to the MOF prepared from ZrCl₄ (SI Figures S138 and S139). Previous work has demonstrated that linkers with polar functional groups can increase the hydrophilicity of MOFs. 62 Thus, the lack of improved hydrophobicity for UiO-66-(OH)2-0.5 M (ZrPiv) is likely due to the two hydroxyl groups on the linker outcompeting the effect of the OPiv defects. Overall, these findings support that both ZrCl₄ and ZrPiv can be used to prepare MOFs at much higher concentrations (0.5-1.0 M) than are typically employed in the literature and that ZrCl₄ is more effective at very high concentrations (1.00 M) at the cost of introducing ordered missing node defects.

Following the same procedure, isoreticular expanded frameworks were also synthesized, namely, UiO-67 and UiO-68-Me₂ (also known as PCN-56) (Figure 6, SI Sections 10 and 11).^{22,69} The synthesis of UiO-67 at high concentrations (Figure 6a) showed comparable results to the functionalized UiO-66 derivatives. Highly crystalline MOF was obtained with ZrCl₄ as the precursor at linker concentrations as high as 1.0 M, while the use of ZrPiv resulted in moderately crystalline MOF at 0.5 M (Figure 6b). Similar results were observed for UiO-68-Me₂ (Figure 6c,d). For both MOFs, the use of ZrPiv with linker concentrations of 1.0 M led to poorly crystalline material (SI Figures S83 and S97). Critically, the BET surface areas of these samples were found to be strongly dependent on the Zr precursor employed. The BET surface area of UiO-67-1.0 M (ZrCl₄) was 2492 \pm 2 m²/g, which is comparable to reported literature values (2250-2824 m²/g),34,70 but the ZrPiv sample had a slightly lower surface area of $1954 \pm 2 \text{ m}^2$ g (Figure 5). Conversely, the surface area of UiO-68-Me₂-1.0 M (ZrCl₄) was only 1237 \pm 7 m²/g, which was drastically lower than the surface area of UiO-68-Me₂-0.5 M (ZrPiv) $(2413 \pm 7 \text{ m}^2/\text{g})$ and the range of reported literature values $(2470-3741 \text{ m}^2/\text{g})$. The BET surface area of UiO-68-Me₂-0.5 M (ZrCl₄) is also much lower than that of UiO-68-Me₂-0.5 M (ZrPiv) (SI Figure S91), indicating that the Zr precursor, not the reaction concentration, is responsible for the differing porosities of the UiO-68-Me2 samples. The low surface areas of UiO-68-Me2 samples prepared from ZrCl4 at high concentrations likely arise from contamination by amorphous coordination polymers. Previous work has

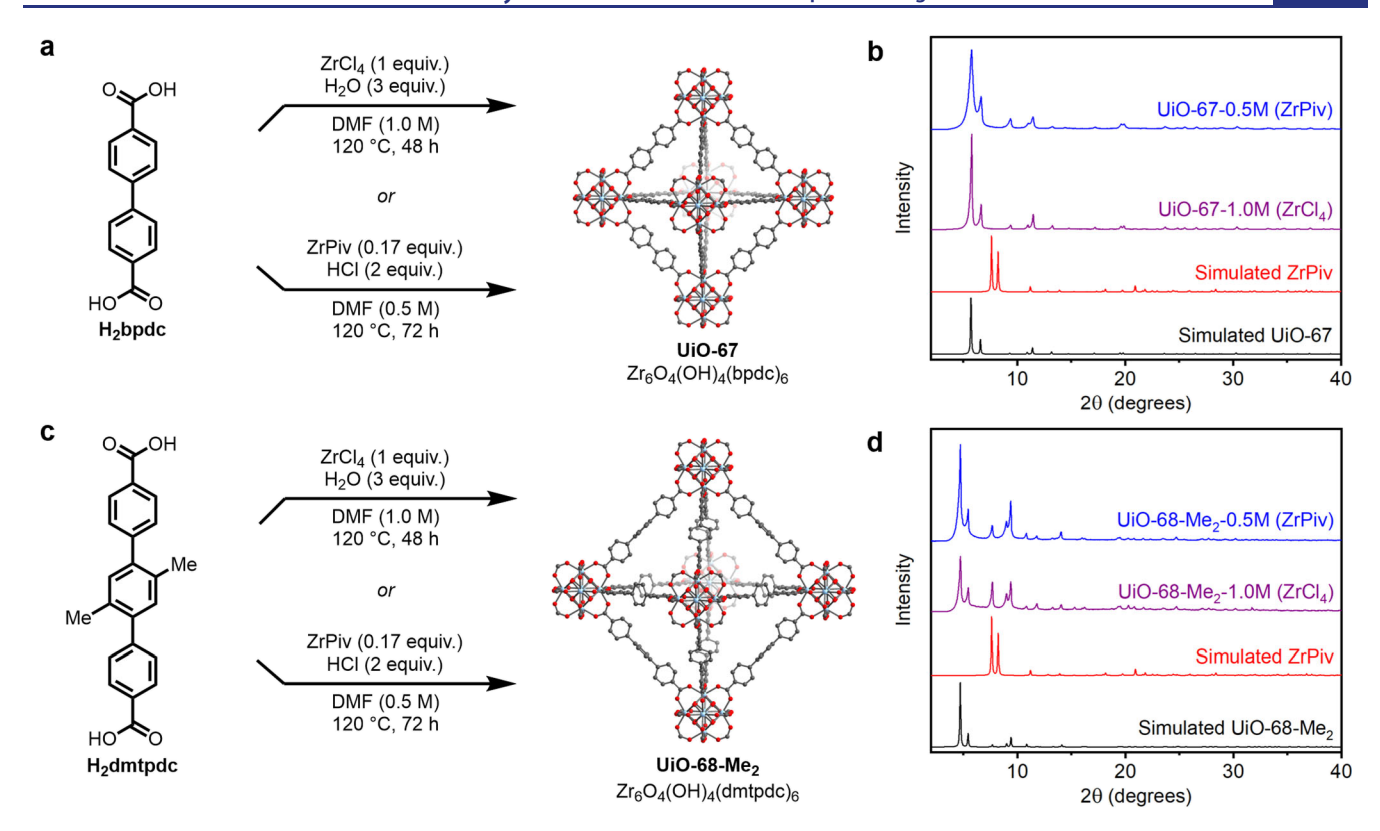


Figure 6. High-concentration syntheses of (a) UiO-67 and (c) UiO-68-Me₂ from either ZrCl₄ or ZrPiv. The gray, red, and light blue spheres represent carbon, oxygen, and zirconium, respectively. Hydrogens are omitted for clarity. PXRD patterns of (b) UiO-67 and (d) UiO-68-Me₂ samples prepared at high concentration from either precursor. The simulated patterns based on the SCXRD structures of ZrPiv, UiO-67, and UiO-68-Me₂ are included for reference. S^{2,69}

demonstrated that acid modulators are required to produce high-quality UiO-68-Me₂.²⁷ Overall, these results demonstrate the utility of a pre-assembled cluster precursor for the high-concentration synthesis of mesoporous MOFs, as standard metal salt precursors resulted in low surface areas for the synthesis of UiO-68-Me₂.

The results outlined above support that Zr- and Hf-MOFs with ditopic, linear linkers can be readily prepared at much higher concentrations (0.5-1.0 M) than are typically employed in the literature (0.01 M). Building upon these results, we investigated whether Zr-MOFs with other topologies can also be prepared at high reaction concentrations. Higher topicity linkers (e.g., 3-4) can generally access multiple framework topologies depending on how many linkers connect to each M₆ node. ²⁰ Zr- and Hf-MOFs with fewer than 12 linkers per node require additional capping ligands, such as monotopic carboxylates, at the remaining coordination sites. We targeted MOF-808, an spn topology MOF composed of tritopic linkers and six-connected nodes, and PCN-128, a csq topology MOF composed of tetratopic linkers and eight-connected nodes,⁷² as mesoporous MOFs to prepare via high-concentration synthesis (Figure 6, SI Sections 12 and 13). MOF-808 is a promising heterogeneous catalyst due to its large 18.4 Å adamantyl cages and readily accessible Lewis-acidic sites, 73 and PCN-128 is useful for enzyme encapsulation due to its massive 44 Å hexagonal channels. It should be noted that neither MOF has been synthesized using mechanochemical methods to date, and our initial attempts to prepare either using LAG were unsuccessful (see SI Section 14 for details). As is standard for their dilute solvothermal syntheses, the addition of a carboxylic acid

modulator—replacing the use of HCl for syntheses with ZrPiv—was found to be necessary for the growth of highly crystalline and phase-pure MOFs.

Following the reported syntheses of MOF-808, 13,73,75 ZrOCl₂·8H₂O was utilized as the standard Zr salt precursor and formic acid was selected to cap the Zr₆ nodes. Trimesic acid (H₃btc) was combined with either ZrOCl₂·8H₂O or ZrPiv in DMF and formic acid (FA) at a linker concentration of 0.5 M in DMF (~0.25 M overall) to yield crystalline MOF-808 samples (Figure 7a,b). The crystallinities of the highconcentration samples were comparable. 77 K N2 adsorption/desorption isotherms revealed that the BET surface areas of MOF-808-0.5 M (ZrOCl₂) and MOF-808-0.5 M (ZrPiv) are 1789 ± 100 and 1732 ± 76 m²/g, respectively (Figure 5), which are comparable to the range of reported literature values (1390–2060 m²/g).^{13,76} Using trifluoroacetic acid (TFA) to cap the Zr_6 nodes, 4',4''',4''''',4''''''-(ethene-1,1,2,2-tetrayl)tetrakis(([1,1'-biphenyl]-4-carboxylic acid)) (H₄ettc) was combined with ZrCl₄ or ZrPiv in DMF at a linker concentration of 0.25 M to yield PCN-128 samples (Figure 6c). This concentration is approximately 30 times higher than the original dilute (0.009 M) synthesis reported for this Synchrotron PXRD of the samples (Figure 6d) revealed that both ZrCl₄ and ZrPiv yield highly crystalline PCN-128, but the ZrCl₄ sample also possesses an additional reflection due to an unidentified impurity. The SEM of PCN-128-0.25 M (ZrCl₄) (SI Figure S116) also contains crystallites of multiple morphologies. In contrast, the sample prepared from ZrPiv exhibits the expected hexagonal rod topology of PCN-128 (SI Figure S124). The BET surface area of the highconcentration PCN-128 sample prepared from ZrCl₄ (1321 ±

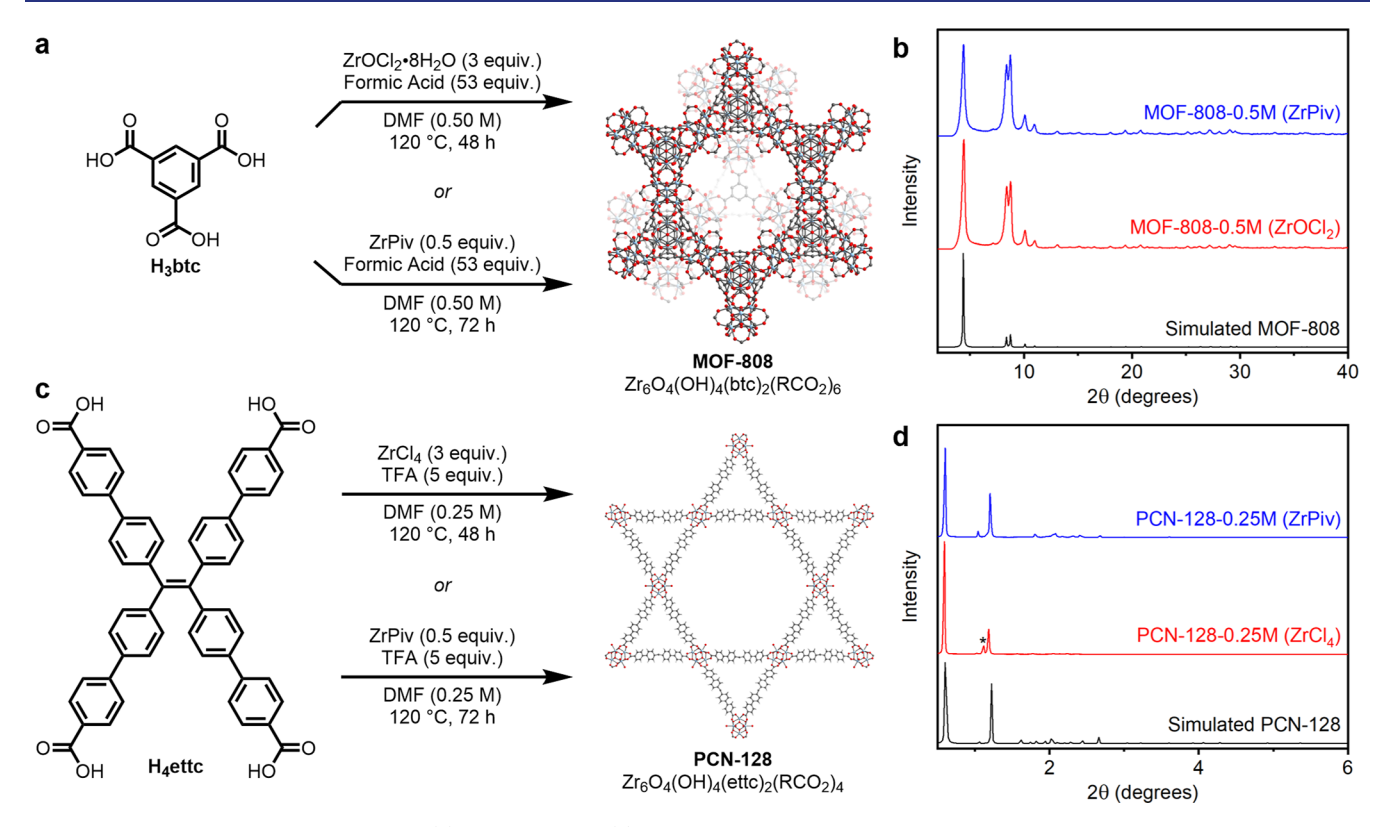


Figure 7. High-concentration syntheses of (a) MOF-808 and (c) PCN-128 from either ZrOCl₂, ZrCl₄, or ZrPiv. TFA represents trifluoroacetic acid. The gray, red, and light blue spheres represent carbon, oxygen, and zirconium, respectively. Hydrogens are omitted for clarity. (b) PXRD patterns of high-concentration MOF-808 samples prepared using either precursor. The simulated pattern based on the SCXRD structure of MOF-808 is included for reference.¹³ (d) Synchrotron PXRD patterns ($\lambda = 0.458949 \text{ Å}$) of high-concentration PCN-128 samples prepared using either precursor. The simulated pattern based on the reported electron diffraction structure of PCN-128 is included for reference.⁷² The asterisk (*) indicates a reflection from an unknown crystalline impurity.

 $8 \text{ m}^2/\text{g}$) was also much lower than that of the ZrPiv prepared sample (1983 \pm 7 m²/g) and reported literature values (2349–2585 m²/g) (Figure 5),^{72,77} likely due to its impurity phase. As such, ZrPiv is a superior precursor for synthesizing high-quality PCN-128.

Despite requiring more capping carboxylates per node, MOF-808-0.5 M (ZrPiv) possesses a lower OPiv⁻:btc³⁻ ratio of 0.14:1 (SI Figure S115) compared to PCN-128-0.25 M (ZrPiv), which has a OPiv-:ettc4- ratio of 0.86:1 (SI Figure S130). The ¹H NMR spectrum of digested MOF-808-0.5 M (ZrPiv) also revealed a large amount of incorporated formate (formate:btc³⁻ ratio of 2.1:1). Thus, the lower OPiv⁻ incorporation for MOF-808 likely arises from the large molar equivalents of FA utilized during MOF synthesis, which displace pivalate groups from the nodes. Additionally, ¹⁹F NMR analysis of digested PCN-128 samples revealed that both contain trifluoroacetate (SI Figures S123 and S131). Consistent with its high degree of OPiv incorporation, PCN-128-0.25 M (ZrPiv) demonstrated increased hydrophobicity (water contact angle of 161°) compared to the sample prepared from ZrCl₄ (SI Figure S143). Overall, the superior results obtained for synthesizing UiO-68-Me2 and PCN-128 from ZrPiv indicate that node assembly is likely a limiting factor during the high-concentration synthesis of largepore MOFs from simple salt precursors.

CONCLUSIONS

Herein, we demonstrate that high-quality Zr- and Hf-MOFs can be prepared solvothermally at 30–100 times higher

concentrations than are typically employed in the literature, challenging the assumption that solvothermal MOF synthesis requires highly dilute reaction conditions. This approach offers a user-friendly alternative to traditional syntheses under dilute conditions as well as to mechanochemical approaches that require specialized equipment (SI Table S1). As such, high-concentration solvothermal synthesis offers a straightforward route for nonspecialists to prepare MOFs for further study. This method, however, despite using less compared to traditional syntheses, still utilizes the hazardous solvent DMF. Future work aims to identify green-solvents compatible with this high-concentration method.

Beyond facilitating MOF synthesis on the benchtop scale, our findings provide insight into MOF self-assembly as well. For smaller pore MOFs, the use of pre-assembled M₆ nodes over metal salt precursors leads to slower MOF assembly but fewer ordered missing node defects. Nonetheless, the final surface areas of small-pore MOFs prepared from either precursor were comparable, indicating that MOF self-assembly occurs efficiently in both cases. In contrast, for two of the largest pore MOFs studied herein, UiO-68-Me, and PCN-128, much higher surface areas were obtained using pre-assembled node precursors. This suggests that efficient node assembly may be a limiting factor during the solvothermal synthesis of mesoporous MOFs. In addition, residual pivalate defects were observed in every MOF prepared from pre-assembled node precursors, supporting that MOF formation involves significant (but incomplete) carboxylate exchange at the nodes. These defects improved the surface hydrophobicity of several MOFs

prepared herein, including UiO-66 (Zr and Hf), UiO-66-NH₂, and PCN-128. Future work will focus on controlling the obtained topology and connectivity for MOFs containing higher topicity linkers, such as H₄ettc, to enable selective phase control during high-concentration syntheses and to expand this method other MOFs.

ASSOCIATED CONTENT

Data Availability Statement

The single-crystal X-ray diffraction structures of ZrPiv and HfPiv are available via the Cambridge Crystallographic Data Centre (CCDC Deposition #2247316-2247317).

5 Supporting Information

The Supporting Information is available free of charge at https://pubs.acs.org/doi/10.1021/jacs.3c02787.

General procedures, synthetic details, water contact angle measurements, crystallographic data, and further characterization of all high-concentration samples, including PXRD patterns, surface area data, SEM images, NMR spectra, IR spectra, and TGA data (PDF)

Accession Codes

CCDC 2247316-2247317 contain the supplementary crystallographic data for this paper. These data can be obtained free of charge via www.ccdc.cam.ac.uk/data_request/cif, or by emailing data_request/cif, or by contacting The Cambridge Crystallographic Data Centre, 12 Union Road, Cambridge CB2 1EZ, UK; fax: +44 1223 336033.

AUTHOR INFORMATION

Corresponding Author

Phillip J. Milner — Department of Chemistry and Chemical Biology, Cornell University, Ithaca, New York 14850, United States; orcid.org/0000-0002-2618-013X; Email: pjm347@cornell.edu

Authors

Ronald T. Jerozal — Department of Chemistry and Chemical Biology, Cornell University, Ithaca, New York 14850, United States

Tristan A. Pitt — Department of Chemistry and Chemical Biology, Cornell University, Ithaca, New York 14850, United States

Samantha N. MacMillan — Department of Chemistry and Chemical Biology, Cornell University, Ithaca, New York 14850, United States; orcid.org/0000-0001-6516-1823

Complete contact information is available at: https://pubs.acs.org/10.1021/jacs.3c02787

Notes

The authors declare the following competing financial interest(s): P.J.M. is listed as a co-inventor on several patents related to metal-organic frameworks.

P.J.M. is listed as a co-inventor on several patents related to MOFs.

ACKNOWLEDGMENTS

The development of methods for the scalable synthesis of MOFs was supported by the National Institute of General Medical Sciences of the National Institutes of Health under award number R35GM138165 (R.T.J., T.A.P., P.J.M.). The content is solely the responsibility of the authors and does not

necessarily represent the official views of the National Institutes of Health. This work made use of the Cornell Center for Materials Research Shared Facilities, which are supported through the NSF MRSEC program (DMR-1719875). ¹H and ¹⁹F NMR data were collected on a Bruker INOVA 500 MHz spectrometer that was purchased with support from the National Science Foundation (CHE-1531632). This work made use of the mail-in service at Beamline 11-BM of the Advanced Photon Source. Use of the Advanced Photon Source at Argonne National Laboratory was supported by the U.S. Department of Energy, Office of Science, Office of Basic Energy Sciences, under Contract No. DE-AC02-06CH11357. This work was performed in part at the Cornell NanoScale Facility, a member of the National Nanotechnology Coordinated Infrastructure (NNCI), which is supported by the National Science Foundation (Grant NNCI-2025233).

REFERENCES

- (1) Furukawa, H.; Cordova, K. E.; O'Keeffe, M.; Yaghi, O. M. The Chemistry and Applications of Metal-Organic Frameworks. *Science* **2013**, *341*, 1230444–1230444.
- (2) Bavykina, A.; Kolobov, N.; Khan, I. S.; Bau, J. A.; Ramirez, A.; Gascon, J. Metal—Organic Frameworks in Heterogeneous Catalysis: Recent Progress, New Trends, and Future Perspectives. *Chem. Rev.* **2020**, *120*, 8468–8535.
- (3) Li, H.; Wang, K.; Sun, Y.; Lollar, C. T.; Li, J.; Zhou, H.-C. Recent Advances in Gas Storage and Separation Using Metal—Organic Frameworks. *Mater. Today* **2018**, *21*, 108–121.
- (4) Sabale, S.; Zheng, J.; Vemuri, R. S.; Yu, X.-Y.; McGrail, B. P.; Motkuri, R. K. Recent Advances in Metal-Organic Frameworks for Heterogeneous Catalyzed Organic Transformations. *Synth. Catal. Open Access* **2016**, *01* (), DOI: 10.4172/2574-0431.100005.
- (5) Ren, J.; Dyosiba, X.; Musyoka, N. M.; Langmi, H. W.; Mathe, M.; Liao, S. Review on the Current Practices and Efforts towards Pilot-Scale Production of Metal-Organic Frameworks (MOFs). *Coord. Chem. Rev.* **2017**, 352, 187–219.
- (6) Julien, P. A.; Mottillo, C.; Friščić, T. Metal-Organic Frameworks Meet Scalable and Sustainable Synthesis. *Green Chem.* **2017**, 19, 2729–2747.
- (7) Stock, N.; Biswas, S. Synthesis of Metal-Organic Frameworks (MOFs): Routes to Various MOF Topologies, Morphologies, and Composites. *Chem. Rev.* **2012**, *112*, 933–969.
- (8) Chen, D.; Zhao, J.; Zhang, P.; Dai, S. Mechanochemical Synthesis of Metal-Organic Frameworks. *Polyhedron* **2019**, *162*, 59–64.
- (9) Friščić, T. New Opportunities for Materials Synthesis Using Mechanochemistry. *J. Mater. Chem.* **2010**, *20*, 7599–7605.
- (10) Du Bois, D. R.; Matzger, A. J. Metal—Organic Framework Seeding to Drive Phase Selection and Overcome Synthesis Limitations. *Cryst. Growth Des.* **2022**, *22*, 6379–6383.
- (11) McKinstry, C.; Cussen, E. J.; Fletcher, A. J.; Patwardhan, S. V.; Sefcik, J. Effect of Synthesis Conditions on Formation Pathways of Metal Organic Framework (MOF-5) Crystals. *Cryst. Growth Des.* **2013**, *13*, 5481–5486.
- (12) Siegelman, R. L.; McDonald, T. M.; Gonzalez, M. I.; Martell, J. D.; Milner, P. J.; Mason, J. A.; Berger, A. H.; Bhown, A. S.; Long, J. R. Controlling Cooperative CO₂ Adsorption in Diamine-Appended Mg₂ (Dobpdc) Metal—Organic Frameworks. *J. Am. Chem. Soc.* **2017**, *139*, 10526—10538.
- (13) Furukawa, H.; Gándara, F.; Zhang, Y.-B.; Jiang, J.; Queen, W. L.; Hudson, M. R.; Yaghi, O. M. Water Adsorption in Porous Metal—Organic Frameworks and Related Materials. *J. Am. Chem. Soc.* **2014**, 136, 4369–4381.
- (14) Morelli Venturi, D.; Campana, F.; Marmottini, F.; Costantino, F.; Vaccaro, L. Extensive Screening of Green Solvents for Safe and

- Sustainable UiO-66 Synthesis. ACS Sustainable Chem. Eng. 2020, 8, 17154–17164.
- (15) Reinsch, H.; Bueken, B.; Vermoortele, F.; Stassen, I.; Lieb, A.; Lillerud, K.-P.; De Vos, D. Green Synthesis of Zirconium-MOFs. *CrystEngComm* **2015**, *17*, 4070–4074.
- (16) Li, Q.; Gies, J.; Yu, X.; Gu, Y.; Terfort, A.; Kind, M. Concentration-Dependent Seeding as a Strategy for Fabrication of Densely Packed Surface-Mounted Metal—Organic Frameworks (SURMOF) Layers. *Chem. Eur. J.* **2020**, *26*, 5185—5189.
- (17) Perfecto-Irigaray, M.; Beobide, G.; Castillo, O.; da Silva, I.; García-Lojo, D.; Luque, A.; Mendia, A.; Pérez-Yáñez, S. [Z 6O₄(OH)₄(Benzene-1,4-Dicarboxylato)₆]_n: A Hexagonal Polymorph of UiO-66. *Chem. Commun.* **2019**, *55*, 5954–5957.
- (18) Forster, P. M.; Stock, N.; Cheetham, A. K. A High-Throughput Investigation of the Role of PH, Temperature, Concentration, and Time on the Synthesis of Hybrid Inorganic-Organic Materials. *Angew. Chem., Int. Ed.* **2005**, *44*, 7608–7611.
- (19) Du Bois, D. R.; Wright, K. R.; Bellas, M. K.; Wiesner, N.; Matzger, A. J. Linker Deprotonation and Structural Evolution on the Pathway to MOF-74. *Inorg. Chem.* **2022**, *61*, 4550–4554.
- (20) Chen, Z.; Hanna, S. L.; Redfern, L. R.; Alezi, D.; Islamoglu, T.; Farha, O. K. Reticular Chemistry in the Rational Synthesis of Functional Zirconium Cluster-Based MOFs. *Coord. Chem. Rev.* **2019**, 386, 32–49.
- (21) Bai, Y.; Dou, Y.; Xie, L.-H.; Rutledge, W.; Li, J.-R.; Zhou, H.-C. Zr-Based Metal—Organic Frameworks: Design, Synthesis, Structure, and Applications. *Chem. Soc. Rev.* **2016**, *45*, 2327–2367.
- (22) Cavka, J. H.; Jakobsen, S.; Olsbye, U.; Guillou, N.; Lamberti, C.; Bordiga, S.; Lillerud, K. P. A New Zirconium Inorganic Building Brick Forming Metal Organic Frameworks with Exceptional Stability. *J. Am. Chem. Soc.* **2008**, *130*, 13850–13851.
- (23) Hu, Z.; Nalaparaju, A.; Peng, Y.; Jiang, J.; Zhao, D. Modulated Hydrothermal Synthesis of UiO-66(Hf)-Type Metal—Organic Frameworks for Optimal Carbon Dioxide Separation. *Inorg. Chem.* **2016**, *55*, 1134—1141.
- (24) Rimoldi, M.; Howarth, A. J.; DeStefano, M. R.; Lin, L.; Goswami, S.; Li, P.; Hupp, J. T.; Farha, O. K. Catalytic Zirconium/Hafnium-Based Metal—Organic Frameworks. *ACS Catal.* **2017**, *7*, 997—1014.
- (25) Howarth, A. J.; Liu, Y.; Li, P.; Li, Z.; Wang, T. C.; Hupp, J. T.; Farha, O. K. Chemical, Thermal and Mechanical Stabilities of Metal—Organic Frameworks. *Nat. Rev. Mater.* **2016**, *1*, 15018.
- (26) Sun, Y.; Sun, L.; Feng, D.; Zhou, H.-C. An In Situ One-Pot Synthetic Approach towards Multivariate Zirconium MOFs. *Angew. Chem., Int. Ed.* **2016**, *55*, 6471–6475.
- (27) Chen, F. E.; Pitt, T. A.; Okongo, D. J.; Wetherbee, L. G.; Fuentes-Rivera, J. J.; Milner, P. J. A Structure—Activity Study of Aromatic Acid Modulators for the Synthesis of Zirconium-Based Metal—Organic Frameworks. *Chem. Mater.* **2022**, *34*, 3383—3394.
- (28) Katz, M. J.; Brown, Z. J.; Colón, Y. J.; Siu, P. W.; Scheidt, K. A.; Snurr, R. Q.; Hupp, J. T.; Farha, O. K. A Facile Synthesis of UiO-66, UiO-67 and Their Derivatives. *Chem. Commun.* **2013**, 49, 9449–9451.
- (29) Schaate, A.; Roy, P.; Godt, A.; Lippke, J.; Waltz, F.; Wiebcke, M.; Behrens, P. Modulated Synthesis of Zr-Based Metal-Organic Frameworks: From Nano to Single Crystals. *Chem. Eur. J.* **2011**, *17*, 6643–6651.
- (30) Salvador, F. E.; Miller, V.; Shimada, K.; Wang, C.-H.; Wright, J.; Das, M.; Chen, Y.-P.; Chen, Y.-S.; Sheehan, C.; Xu, W.; Rubasinghege, G.; Gao, W.-Y. Mechanochemistry of Group 4 Element-Based Metal—Organic Frameworks. *Inorg. Chem.* **2021**, *60*, 16079—16084.
- (31) Karadeniz, B.; Žilić, D.; Huskić, I.; Germann, L. S.; Fidelli, A. M.; Muratović, S.; Lončarić, I.; Etter, M.; Dinnebier, R. E.; Barišić, D.; Cindro, N.; Islamoglu, T.; Farha, O. K.; Friščić, T.; Užarević, K. Controlling the Polymorphism and Topology Transformation in Porphyrinic Zirconium Metal—Organic Frameworks via Mechanochemistry. *J. Am. Chem. Soc.* 2019, 141, 19214—19220.

- (32) Karadeniz, B.; Howarth, A. J.; Stolar, T.; Islamoglu, T.; Dejanović, I.; Tireli, M.; Wasson, M. C.; Moon, S.-Y.; Farha, O. K.; Friščić, T.; Užarević, K. Benign by Design: Green and Scalable Synthesis of Zirconium UiO-Metal—Organic Frameworks by Water-Assisted Mechanochemistry. ACS Sustainable Chem. Eng. 2018, 6, 15841—15849.
- (33) Užarević, K.; Wang, T. C.; Moon, S.-Y.; Fidelli, A. M.; Hupp, J. T.; Farha, O. K.; Friščić, T. Mechanochemical and Solvent-Free Assembly of Zirconium-Based Metal—Organic Frameworks. *Chem. Commun.* **2016**, *52*, 2133—2136.
- (34) Fidelli, A. M.; Karadeniz, B.; Howarth, A. J.; Huskić, I.; Germann, L. S.; Halasz, I.; Etter, M.; Moon, S.-Y.; Dinnebier, R. E.; Stilinović, V.; Farha, O. K.; Friščić, T.; Užarević, K. Green and Rapid Mechanosynthesis of High-Porosity NU- and UiO-Type Metal-Organic Frameworks. *Chem. Commun.* **2018**, *54*, 6999–7002.
- (35) Ali-Moussa, H.; Navarro Amador, R.; Martinez, J.; Lamaty, F.; Carboni, M.; Bantreil, X. Synthesis and Post-Synthetic Modification of UiO-67 Type Metal-Organic Frameworks by Mechanochemistry. *Mater. Lett.* **2017**, *197*, 171–174.
- (36) Huang, Y.-H.; Lo, W.-S.; Kuo, Y.-W.; Chen, W.-J.; Lin, C.-H.; Shieh, F.-K. Green and Rapid Synthesis of Zirconium Metal—Organic Frameworks via Mechanochemistry: UiO-66 Analog Nanocrystals Obtained in One Hundred Seconds. *Chem. Commun.* **2017**, *53*, 5818–5821.
- (37) Xu, H.; Sommer, S.; Broge, N. L. N.; Gao, J.; Iversen, B. B. The Chemistry of Nucleation: In Situ Pair Distribution Function Analysis of Secondary Building Units During UiO-66 MOF Formation. *Chem. Eur. J.* **2019**, *25*, 2051–2058.
- (38) D'Amato, R.; Bondi, R.; Moghdad, I.; Marmottini, F.; McPherson, M. J.; Naïli, H.; Taddei, M.; Costantino, F. "Shake 'n Bake" Route to Functionalized Zr-UiO-66 Metal—Organic Frameworks. *Inorg. Chem.* **2021**, *60*, 14294—14301.
- (39) Zhang, Y.; de Azambuja, F.; Parac-Vogt, T. N. The Forgotten Chemistry of Group(IV) Metals: A Survey on the Synthesis, Structure, and Properties of Discrete Zr(IV), Hf(IV), and Ti(IV) Oxo Clusters. *Coord. Chem. Rev.* **2021**, 438, No. 213886.
- (40) Guillerm, V.; Gross, S.; Serre, C.; Devic, T.; Bauer, M.; Férey, G. A Zirconium Methacrylate Oxocluster as Precursor for the Low-Temperature Synthesis of Porous Zirconium(IV) Dicarboxylates. *Chem. Commun.* **2010**, *46*, 767–769.
- (41) DeStefano, M. R.; Islamoglu, T.; Garibay, S. J.; Hupp, J. T.; Farha, O. K. Room-Temperature Synthesis of UiO-66 and Thermal Modulation of Densities of Defect Sites. *Chem. Mater.* **2017**, *29*, 1357–1361.
- (42) Puchberger, M.; Kogler, F. R.; Jupa, M.; Gross, S.; Fric, H.; Kickelbick, G.; Schubert, U. Can the Clusters $\mathrm{Zr}_6O_4(\mathrm{OH})_4(\mathrm{OOCR})_{12}$ and $[\mathrm{Zr}_6O_4(\mathrm{OH})_4(\mathrm{OOCR})_{12}]_2$ Be Converted into Each Other? *Eur. J. Inorg. Chem.* **2006**, 2006, 3283–3293.
- (43) Kreutzer, J.; Puchberger, M.; Artner, C.; Schubert, U. Retention of the Cluster Core Structure during Ligand Exchange Reactions of Carboxylato-Substituted Metal Oxo Clusters. *Eur. J. Inorg. Chem.* **2015**, 2015, 2145–2151.
- (44) Cliffe, M. J.; Castillo-Martínez, E.; Wu, Y.; Lee, J.; Forse, A. C.; Firth, F. C. N.; Moghadam, P. Z.; Fairen-Jimenez, D.; Gaultois, M. W.; Hill, J. A.; Magdysyuk, O. V.; Slater, B.; Goodwin, A. L.; Grey, C. P. Metal—Organic Nanosheets Formed via Defect-Mediated Transformation of a Hafnium Metal—Organic Framework. *J. Am. Chem. Soc.* 2017, 139, 5397—5404.
- (45) Ji, P.; Manna, K.; Lin, Z.; Feng, X.; Urban, A.; Song, Y.; Lin, W. Single-Site Cobalt Catalysts at New $Zr_{12}(\mu_3-O)_8(\mu_3-OH)_8(\mu_2-OH)_6$ Metal—Organic Framework Nodes for Highly Active Hydrogenation of Nitroarenes, Nitriles, and Isocyanides. *J. Am. Chem. Soc.* **2017**, *139*, 7004–7011.
- (46) Ermer, M.; Mehler, J.; Kriesten, M.; Avadhut, Y. S.; Schulz, P. S.; Hartmann, M. Synthesis of the Novel MOF Hcp UiO-66 Employing Ionic Liquids as a Linker Precursor. *Dalton Trans.* **2018**, 47, 14426–14430.
- (47) Bezrukov, A. A.; Törnroos, K. W.; Le Roux, E.; Dietzel, P. D. C. Incorporation of an Intact Dimeric Zr12 Oxo Cluster from a

- Molecular Precursor in a New Zirconium Metal-Organic Framework. Chem. Commun. 2018, 54, 2735-2738.
- (48) Van den Eynden, D.; Pokratath, R.; Mathew, J. P.; Goossens, E.; De Buysser, K.; De Roo, J. Fatty Acid Capped, Metal Oxo Clusters as the Smallest Conceivable Nanocrystal Prototypes. Chem. Sci. 2023, 14, 573-585.
- (49) Piszczek, P.; Radtke, A.; Grodzicki, A.; Wojtczak, A.; Chojnacki, J. The New Type of $[Zr_6(\mu_3-O)_4(\mu_3-OH)_4]$ Cluster Core: Crystal Structure and Spectral Characterization of [Zr₆O₄(OH)₄(OOCR)₁₂] $(R=Bu^t, C(CH_3)_2Et)$. Polyhedron **2007**, 26, 679–685.
- (50) Liu, B.; Vellingiri, K.; Jo, S.-H.; Kumar, P.; Ok, Y. S.; Kim, K.-H. Recent Advances in Controlled Modification of the Size and Morphology of Metal-Organic Frameworks. Nano Res. 2018, 11, 4441-4467.
- (51) Howarth, A. J.; Peters, A. W.; Vermeulen, N. A.; Wang, T. C.; Hupp, J. T.; Farha, O. K. Best Practices for the Synthesis, Activation, and Characterization of Metal-Organic Frameworks. Chem. Mater. 2017, 29, 26-39.
- (52) Øien, S.; Wragg, D.; Reinsch, H.; Svelle, S.; Bordiga, S.; Lamberti, C.; Lillerud, K. P. Detailed Structure Analysis of Atomic Positions and Defects in Zirconium Metal-Organic Frameworks. Cryst. Growth Des. 2014, 14, 5370-5372.
- (53) Cliffe, M. J.; Wan, W.; Zou, X.; Chater, P. A.; Kleppe, A. K.; Tucker, M. G.; Wilhelm, H.; Funnell, N. P.; Coudert, F.-X.; Goodwin, A. L. Correlated Defect Nanoregions in a Metal-Organic Framework. Nat. Commun. 2014, 5, 4176.
- (54) Shearer, G. C.; Chavan, S.; Bordiga, S.; Svelle, S.; Olsbye, U.; Lillerud, K. P. Defect Engineering: Tuning the Porosity and Composition of the Metal-Organic Framework UiO-66 via Modulated Synthesis. Chem. Mater. 2016, 28, 3749-3761.
- (55) Matemb Ma Ntep, T.; Breitzke, H.; Schmolke, L.; Schlüsener, C.; Moll, B.; Millan, S.; Tannert, N.; El Aita, I.; Buntkowsky, G.; Janiak, C. Facile in Situ Halogen Functionalization via Triple-Bond Hydrohalogenation: Enhancing Sorption Capacities through Halogenation to Halofumarate-Based Zr(IV)-Metal-Organic Frameworks. Chem. Mater. 2019, 31, 8629-8638.
- (56) Athar, M.; Rzepka, P.; Thoeny, D.; Ranocchiari, M.; Anton van Bokhoven, J. Thermal Degradation of Defective High-Surface-Area UiO-66 in Different Gaseous Environments. RSC Adv. 2021, 11, 38849-38855.
- (57) Atzori, C.; Shearer, G. C.; Maschio, L.; Civalleri, B.; Bonino, F.; Lamberti, C.; Svelle, S.; Lillerud, K. P.; Bordiga, S. Effect of Benzoic Acid as a Modulator in the Structure of UiO-66: An Experimental and Computational Study. J. Phys. Chem. C 2017, 121, 9312-9324.
- (58) Wang, Z.; Bilegsaikhan, A.; Jerozal, R. T.; Pitt, T. A.; Milner, P. J. Evaluating the Robustness of Metal-Organic Frameworks for Synthetic Chemistry. ACS Appl. Mater. Interfaces 2021, 13, 17517-
- (59) Xie, L.-H.; Liu, X.-M.; He, T.; Li, J.-R. Metal-Organic Frameworks for the Capture of Trace Aromatic Volatile Organic Compounds. Chem 2018, 4, 1911-1927.
- (60) Rao, K. P.; Higuchi, M.; Sumida, K.; Furukawa, S.; Duan, J.; Kitagawa, S. Design of Superhydrophobic Porous Coordination Polymers through the Introduction of External Surface Corrugation by the Use of an Aromatic Hydrocarbon Building Unit. Angew. Chem., Int. Ed. 2014, 53, 8225-8230.
- (61) Canivet, J.; Bonnefoy, J.; Daniel, C.; Legrand, A.; Coasne, B.; Farrusseng, D. Structure-Property Relationships of Water Adsorption in Metal-Organic Frameworks. New J. Chem. 2014, 38, 3102-3111.
- (62) Cmarik, G. E.; Kim, M.; Cohen, S. M.; Walton, K. S. Tuning the Adsorption Properties of UiO-66 via Ligand Functionalization. Langmuir 2012, 28, 15606-15613.
- (63) Kandiah, M.; Nilsen, M. H.; Usseglio, S.; Jakobsen, S.; Olsbye, U.; Tilset, M.; Larabi, C.; Quadrelli, E. A.; Bonino, F.; Lillerud, K. P. Synthesis and Stability of Tagged UiO-66 Zr-MOFs. Chem. Mater. 2010, 22, 6632-6640.
- (64) DeKrafft, K. E.; Boyle, W. S.; Burk, L. M.; Zhou, O. Z.; Lin, W. Zr- and Hf-Based Nanoscale Metal-Organic Frameworks as Contrast

- Agents for Computed Tomography. J. Mater. Chem. 2012, 22, 18139-18144.
- (65) Sun, C. G. C.; Neufeld, M. J.; Duross, A. N. Nanoscale Metal-Organic Frameworks For Enhanced Tumor Chemoradiation. US2021115071A1. 2021
- (66) Jakobsen, S.; Gianolio, D.; Wragg, D. S.; Nilsen, M. H.; Emerich, H.; Bordiga, S.; Lamberti, C.; Olsbye, U.; Tilset, M.; Lillerud, K. P. Structural Determination of a Highly Stable Metal-Organic Framework with Possible Application to Interim Radioactive Waste Scavenging: Hf-UiO-66. Phys. Rev. B 2012, 86, No. 125429.
- (67) Bakuru, V. R.; Churipard, S. R.; Maradur, S. P.; Kalidindi, S. B. Exploring the Brønsted Acidity of UiO-66 (Zr, Ce, Hf) Metal-Organic Frameworks for Efficient Solketal Synthesis from Glycerol Acetalization. Dalton Trans. 2019, 48, 843-847.
- (68) Rada, Z. H.; Abid, H. R.; Shang, J.; Sun, H.; He, Y.; Webley, P.; Liu, S.; Wang, S. Functionalized UiO-66 by Single and Binary (OH)2 and NO₂ Groups for Uptake of CO₂ and CH₄. Ind. Eng. Chem. Res. **2016**, *55*, 7924–7932.
- (69) Jiang, H.-L.; Feng, D.; Liu, T.-F.; Li, J.-R.; Zhou, H.-C. Pore Surface Engineering with Controlled Loadings of Functional Groups via Click Chemistry in Highly Stable Metal-Organic Frameworks. J. Am. Chem. Soc. 2012, 134, 14690-14693.
- (70) Shalini, S.; Vaid, T. P.; Matzger, A. J. Salt Nanoconfinement in Zirconium-Based Metal-Organic Frameworks Leads to Pore-Size and Loading-Dependent Ionic Conductivity Enhancement. Chem. Commun. 2020, 56, 7245-7248.
- (71) Carson, F.; Martínez-Castro, E.; Marcos, R.; Miera, G. G.; Jansson, K.; Zou, X.; Martín-Matute, B. Effect of the Functionalisation Route on a Zr-MOF with an Ir-NHC Complex for Catalysis. Chem. Commun. 2015, 51, 10864-10867.
- (72) Zhang, Q.; Su, J.; Feng, D.; Wei, Z.; Zou, X.; Zhou, H.-C. Piezofluorochromic Metal-Organic Framework: A Microscissor Lift. J. Am. Chem. Soc. 2015, 137, 10064-10067.
- (73) Ly, H. G. T.; Fu, G.; Kondinski, A.; Bueken, B.; De Vos, D.; Parac-Vogt, T. N. Superactivity of MOF-808 toward Peptide Bond Hydrolysis. J. Am. Chem. Soc. 2018, 140, 6325-6335.
- (74) Li, P.; Moon, S.-Y.; Guelta, M. A.; Harvey, S. P.; Hupp, J. T.; Farha, O. K. Encapsulation of a Nerve Agent Detoxifying Enzyme by a Mesoporous Zirconium Metal-Organic Framework Engenders Thermal and Long-Term Stability. J. Am. Chem. Soc. 2016, 138,
- (75) Jiang, J.; Gándara, F.; Zhang, Y.-B.; Na, K.; Yaghi, O. M.; Klemperer, W. G. Superacidity in Sulfated Metal-Organic Framework-808. J. Am. Chem. Soc. 2014, 136, 12844-12847.
- (76) Zheng, H.-Q.; Liu, C.-Y.; Zeng, X.-Y.; Chen, J.; Lü, J.; Lin, R.-G.; Cao, R.; Lin, Z.-J.; Su, J.-W. MOF-808: A Metal-Organic Framework with Intrinsic Peroxidase-Like Catalytic Activity at Neutral PH for Colorimetric Biosensing. Inorg. Chem. 2018, 57, 9096-9104.
- (77) Tai, T.-Y.; Sha, F.; Wang, X.; Wang, X.; Ma, K.; Kirlikovali, K. O.; Su, S.; Islamoglu, T.; Kato, S.; Farha, O. K. Leveraging Isothermal Titration Calorimetry to Explore Structure-Property Relationships of Protein Immobilization in Metal-Organic Frameworks. Angew. Chem., Int. Ed. 2022, 61, No. e202209110.